Journal of ELECTRONIC MATERIALS, Vol. 49, No. 11, 2020
https://doi.org/10.1007/s11664-020-08414-1

Modifying the Soft Magnetic Properties of Mn-Zn Ferrites by Ce_2O_3-Doping and Sintering Temperature Optimization

JINGWEN HU,[1] ZHAOYU LI,[1] HONGYA YU,[1,2] XICHUN ZHONG,[1,2] ZHONGWU LIU ,[1,2,4] KEWEN LONG,[2] and JING LI[3,5]

1.—School of Materials Science and Engineering, South China University of Technology, Guangzhou 510640, China. 2.—Sanqiaohui (Foshan) New Materials Co., Ltd, Foshan 528200, China. 3.—School of Chemistry and Chemical Engineering, South China University of Technology, Guangzhou 510640, China. 4.—e-mail: zwliu@scut.edu.cn. 5.—e-mail: ljing@scut.edu.cn

Abundant rare earth-based Ce_2O_3 was employed as the doping for improving the magnetic performance of low-cost Mn-Zn ferrites. To achieve the best doping effect, the influence of sintering temperature on the microstructure and magnetic properties was also investigated. Based on the characterization of the samples prepared at different sintering temperatures (1250–1350°C) and with various Ce_2O_3 contents (0–0.05 wt.%), it has been found that the magnetic properties are determined by the grain size, the distribution of the pores, and the internal stress associated with impurities. The amplitude permeability for the samples with small grains shows good frequency stability in the range of 10–100 kHz. Increasing the sintering temperature or doping a certain amount of Ce_2O_3 can increase the amplitude permeability and reduce the magnetic loss of the ferrite. However, excessive Ce addition or excessive sintering temperature led to increasing magnetic loss. For the sample doped with 0.01 wt.% Ce_2O_3, the maximum amplitude permeabilities of 4105 (20 kHz and 100 mT) and 2830 (100 kHz, 100 mT) can be obtained when sintered at 1350°C, while the minimum power loss with 5.4 W/kg (20 kHz, 100 mT) and 46 W/kg (100 kHz, 100 mT) can be achieved at a sintering temperature of 1280°C. The present results indicate that Ce doping cannot only effectively increase the amplitude permeability and decrease the magnetic loss but can also reduce the sintering temperature. The produced ferrites show great potential for the applications in induction heating systems and other fields.

Key words: Mn-Zn ferrites, Ce_2O_3-doping, sintering temperature, magnetic properties, microstructure

INTRODUCTION

The well-known Mn-Zn ferrites exhibit good soft magnetic properties with high electric resistivity, high saturation magnetization, low loss, and high permeability. They are widely used in various low- and high-frequency devices such as transformers, multilayered chip inductors, sensors, information storage systems, information communications, and magnetic diagnostics.[1–4] With the rapid development of the electric and electronic industries, Mn-Zn ferrites with further improved properties, such as higher permeability and lower loss, are still required in response to the miniaturization, light weight, and multifunction of electronic devices.[5] For example, Mn-Zn ferrites are used in electromagnetic induction heating as magnetic strips. To improve the heating efficiency, high permeability and low magnetic loss at 10–100 kHz are required. In addition to the composition and process,

(Received March 25, 2020; accepted August 13, 2020; published online August 28, 2020)

additives have important influences on the performance of Mn-Zn ferrites.[6] Hence, element doping is an important way to modify their electromagnetic properties.

Recently, rare earth (RE) elements have received much attention from ferrite industries.[6,7] Different kinds of RE elements, such as gadolinium (Gd),[8] dysprosium (Dy),[9,10] neodymium (Nd),[11] samarium (Sm),[12–16] lanthanum (La),[17] terbium (Tb),[10,18,19] cerium (Ce),[18,20–22] etc., have been introduced into different types of ferrites. The obtained results reveal that, by introducing a small amount of RE_2O_3 to substitute Fe_2O_3, modifications of both the structure and the magnetic properties can be obtained. With optimized doping contents, the magnetic properties of ferrites can be improved. Also, it has been observed that ferrites synthesized by different methods exhibit different microstructures, including local phase precipitation, domain structure, and grain size, which determine the final properties.[12,23] As a result, the effects of RE doping on the ferrites also depend on the preparation method.

As is known, the heavy RE elements, such as Dy and Tb, are rare and expensive, and Nd, Pr, and Sm are also critical elements for RE magnets. Using abundant RE elements, like Ce and La, is thus desirable for improving the properties and maintaining the low cost of the ferrites. For nano-sized nickel zinc ferrite, Sonia et al.[24] reported that the coercivity can be reduced from 159 Oe for $NiFe_2O_4$ to 101 Oe for $NiCe_{0.1}Fe_{1.9}O_4$ by Ce doping. Dar et al.[25] reported the high value of M_s = 123 emu/g for $Ni_{0.5}Zn_{0.5}Fe_{1.96}Ce_{0.04}O_4$. However, up to now, there has not been much work on Ce-substituted Mn-Zn ferrites prepared by traditional sintering methods. In addition, since the composition is closely associated with the optimized process of ferrites, for ferrites with different RE doping, the preparation process should be modified accordingly in order to achieve the best electromagnetic performance.

In this work, the structural and magnetic properties of Mn-Zn ferrites prepared by a ceramic process and doped with various Ce_2O_3 contents were analyzed. These ferrites are designed as magnetic strips in induction heating systems. The effects of the sintering temperature, one of the most important processing parameters, were also investigated. The results suggest that the soft magnetic properties could be modified by both composition and process optimization.

EXPERIMENTAL

The Mn-Zn ferrites were prepared via a conventional ceramic process. The raw oxides, including Fe_2O_3 (purity ≥ 99.0%), MnO_2 (purity ≥ 85.0%) , and ZnO (purity ≥ 99.0%) were mixed by a wet-milling method in stoichiometric molar ratio with Fe_2O_3:MnO_2:ZnO = 52.7:32.6:14.8. The obtained powders were pre-sintered at 920°C for 2 h in air. Then pre-sintered powders with added 0.05 wt.% $CaCO_3$ and various amounts of Ce_2O (0 wt.%, 0.01 wt.%, 0.03 wt.%, 0.05 wt.%) were wet-milled for 4 h with the weight ratios of ball, powder, and water of 4:1:1. The mixed powders were granulated into particles with diameters between 120 μm and 180 μm by adding 10 wt.% polyvinyl alcohol solution as a binder. The granulated particles were then pressed into toroid-shape samples with an external diameter of 20 mm, internal diameter of 12 mm, and height of 4 mm under a pressure of 100 MPa. Finally, the samples were sintered at various temperatures from 1250°C to 1350°C for 3 h under a 4 wt.%O_2 + N_2 atmosphere, followed by cooling in a pure nitrogen atmosphere.

The phase constitution of the samples was characterized by θ–2θ, x-ray diffraction with Cu-$K_{\alpha 1}$ (λ = 0.1540598 nm) at room temperature using a Philips X'Pert MPD x-ray diffractometer. The microstructure of the samples was observed using an optical microscope (DMI 3000 M). The magnetic properties including amplitude permeability, magnetic loss, and coercivity were tested by a soft magnetic measuring device (MATS-2010SA; Hunan Linkjoin Technology) at 100 mT and 10–100 kHz. The initial permeability was measured by an LCR tester (HIOKI IM3536) with a magnetic induction $B \leq 0.25$ mT at a frequency of 10 kHz.

RESULTS AND DISCUSSION

Structure Analysis

The XRD patterns of the Mn-Zn ferrite samples with different Ce_2O_3 contents and sintered at 1250°C and 1350°C are shown in Fig. 1. Even when the sintering temperature is 1250°C, there is no Fe_2O_3 diffraction peak observed, indicating that the oxides have completely reacted to the Mn-Zn ferrite at sintering temperatures of 1250–1350°C. All the samples show a single spinel ferrite phase structure, and no significant diffraction peaks from other phases are observed, indicating a relatively pure

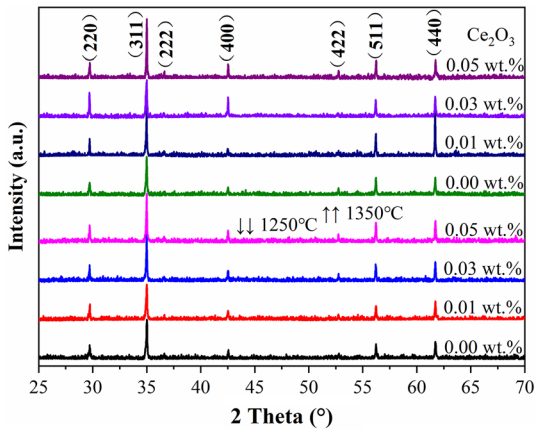

Fig. 1. XRD patterns for the Mn-Zn ferrite samples doped with various Ce_2O_3 sintered at 1250°C and 1350°C.

Mn-Zn ferrite phase. The main diffraction peaks of the samples with different Ce_2O_3 additions do not shift significantly, implying that doping by 0.05 wt.% $CaCO_3$ and 0–0.05 wt.% Ce_2O_3 has no significant effect on the crystal structure of the Mn-Zn ferrite and does not lead to significant lattice distortion or lattice expansion. A Ca^{2+}-containing impurity was not detected either, indicating that possible impurities such as $CeFeO_3$ or $CaO{\cdot}Fe_2O_3$ are very few. The samples prepared at other sintering temperatures show similar results, which are not shown here.

Microstructure Analysis

Figure 2 shows the metallographic images for all the samples with different Ce_2O_3 contents prepared at various sintering temperatures. Table I shows the average grain sizes of the samples. The results show that the grain size increases with the increase of sintering temperature or Ce_2O_3 content. As is known, the solid-state reaction of ferrites prepared by ceramics is mainly controlled by the element diffusion. According to the diffusion kinetics and thermodynamics, a high temperature leads to a high internal energy of the atoms and the fast thermal movement of the molecules, which results in a large diffusion coefficient and a fast grain growth rate. At the same time, Ce_2O_3 doping effectively promotes the grain growth. The reason is as follows. The common valence of the Ce ion is + 3 or + 4 with ionization energies of 1949 kJ/mol or 3547 kJ/mol, respectively. A part of the Ce may enter the ferrite lattice in the form of Ce^{4+} with an ionic radius of 0.092 nm, similar to the Ti^{4+} with an ionic radius of 0.068 nm and ionization energy of 4174.6 kJ/mol.[26] The excess cation vacancies increase the pore mobility, similar to that by adding titanium dioxide. As is known, the migration rate of the grain boundaries with adherent pores increases with the increase of pore mobility. The cation vacancy flux generated by Ce^{4+} diffusion increases the pore mobility and thus the mobility of pore-loaded grain boundaries. In addition, it is also possible that some of the Ce precipitate at the grain boundaries in the form of Ce^{3+} (ion radius 0.103 nm), which can promote CaO and Fe_2O_3 to

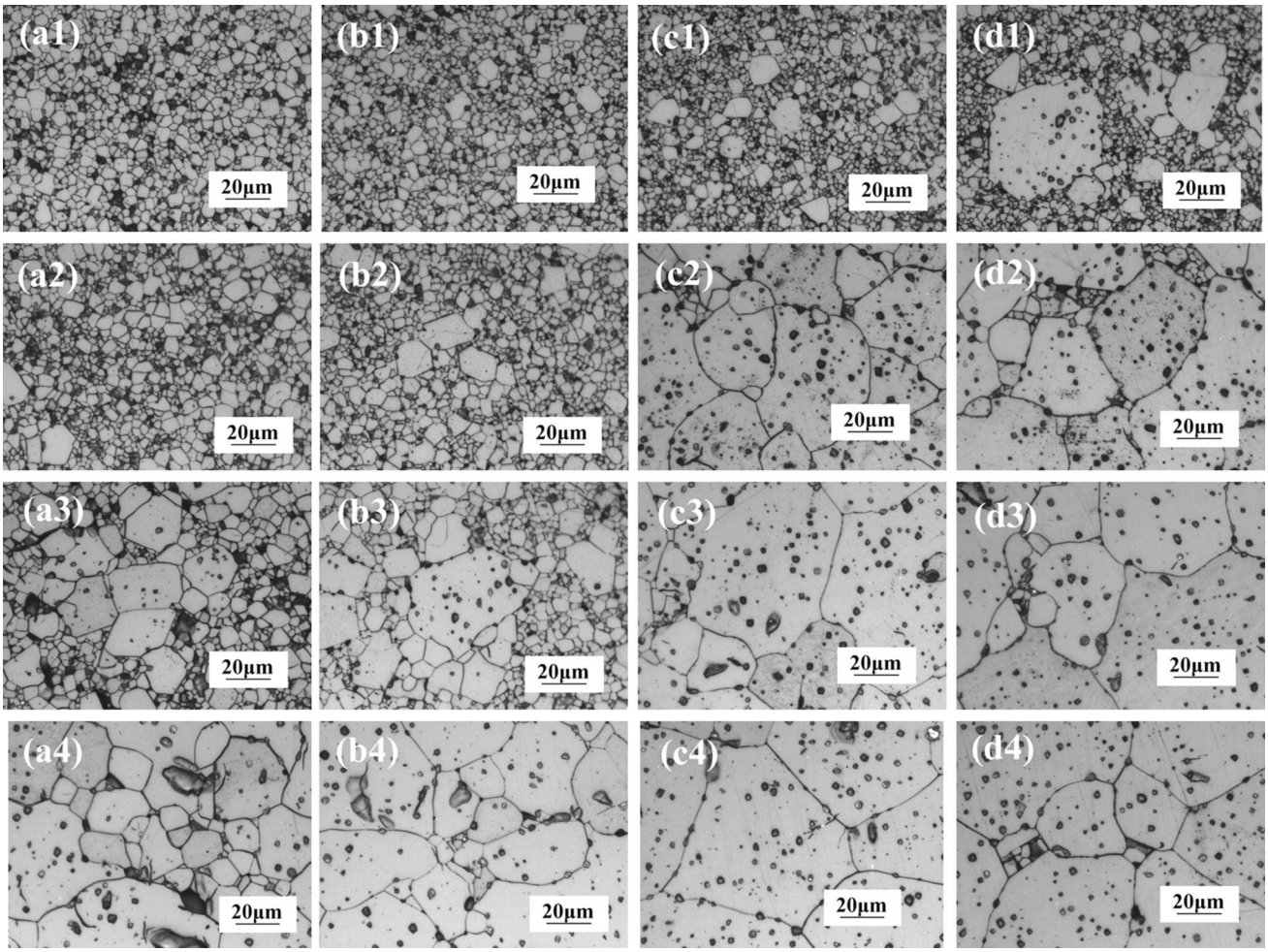

Fig. 2. Metallographic images for the Mn-Zn ferrite samples with various Ce_2O_3 doping sintered at various temperatures: (a) 0.00 wt.%; (b) 0.01 wt.%; (c) 0.03 wt.%; (d) 0.05 wt.%. (1) 1250°C; (2) 1280°C; (3) 1300°C; (4) 1350°C.

Table I. The average grain sizes of Mn-Zn ferrites with various Ce_2O_3 doping sintered at various temperatures

	Grain size, μm			
Sintering temperature, °C	**0.00 wt.%**	**0.01 wt.%**	**0.03 wt.%**	**0.05 wt.%**
1250°C	3.0–3.5	3.5–4.0	4.0–4.5	5.5–6.0
1280°C	3.5–4.0	4.0–4.5	25–30	35–40
1300°C	7–8	9–10	40–45	45–50
1350°C	20–25	25–30	> 60	> 60

form eutectic compounds with low melting points[26] beneficial for liquid phase sintering. This also explains the phenomenon that the local coarse grains are surrounded by fine grains in the samples with 0.03 wt.% or 0.05 wt.% Ce_2O_3 sintered at 1250°C, as shown in Fig. 2c1 and d1, respectively.

Figure 2 also shows that all the samples have uniform pore distributions. However, the specific location of the pores is closely related to the grain size. For the samples with the grain size below 10 μm, there are almost no pores inside the grains, and the pores are mainly distributed at the grain boundary, especially at the junction of triple points. For the samples with grains larger than 10 μm, there are some pores inside the grains. The larger the grain size, the more pores are inside the grain. This phenomenon can be explained based on the grain growth rate. An excessive growth rate of the grains or high-temperature liquid-phase sintering causes difficulties in the discharge of the gas in the pores. As a result, the gas remains inside the grains, and thus a large number of pores are retained inside the grains. The existence of porosity may lead to the generation of stress. During high-temperature sintering, without considering the interfacial tension, the pressures inside and outside the pores keep a dynamic equilibrium, hence the stress inside the grains is about zero. However, the thermal expansion coefficient of the gas is much larger than that of the Mn-Zn ferrite. During the cooling process, the pores shrink dramatically. If the pressure inside and outside the pores still keeps a dynamic equilibrium, the grains near the pores are subjected to significant tensile stress, which is not beneficial for the soft magnetic properties. For an appropriate grain growth rate, the grain size is small, and the pores have more time to drain out along the grain boundaries during the densification process. As a result, there are fewer pores inside the grains, and the residual pores tend to distribute at the grain boundaries, especially at the junction of triple grains. Although the grains near the pores are also subjected to tensile stress, these pores have little influence on the grain interior as most of them are distributed at grain boundaries.

Magnetic Properties

The initial permeabilities μ_I and the saturation magnetic induction B_s of the samples with different Ce_2O_3 contents prepared at various sintering temperatures are shown in Fig. 3a and b, respectively. It can be observed that, for most of the samples, B_s increases with the increase of sintering temperature. The B_s for the sample sintered at 1250°C and 1280°C increases with the increase of the Ce_2O_3 addition. However, for the sample sintered at 1300°C and 1350°C, the B_s shows a maximum value at a certain Ce_2O_3 content. The μ_I for the sample sintered at 1350°C decreases with the increase of the Ce_2O_3 addition, but, for other samples sintered at 1250–1300°C, μ_I increases for the Ce_2O_3 content of 0.01 wt.%, and decreases with the further increase of the addition. For the samples with identical Ce_2O_3 contents, the higher sintering temperature leads to a higher μ_I, except for the sample with 0.01 wt.% Ce_2O_3 sintered at 1300°C.

As is well known, the permeability of magnetic materials is greatly influenced by the porosity, impurity concentration, and internal stress. The relationship between initial permeability and various factors can be expressed as follows:

$$\mu_I \propto \frac{\mu_0 M_s^2 D}{[|K_1| + (3/2)\lambda_s \sigma]\beta^{1/3}\delta} \quad (1)$$

Equation (1) shows that μ_I is proportional to the grain size D and the square of the saturation magnetization M_s^2, and inversely proportional to the anisotropy constant K_1, the magnetostriction coefficient $_s$, the interior stress σ, the cubic root of the volume concentration of impurities (including pores) $\beta^{1/3}$, and the domain wall thickness δ. The magnetization mechanism, which determines the value of μ_I, varies with the grain size. When the grain size is small, the magnetization mechanism is dominated by the magnetization rotation, and hence the μ_I is relatively low.[27] For the samples with large grains, the barrier of the grain boundary to the domain wall displacement is small. As a result, μ_I increases with the increase of grain size, as demonstrated by our experiments.

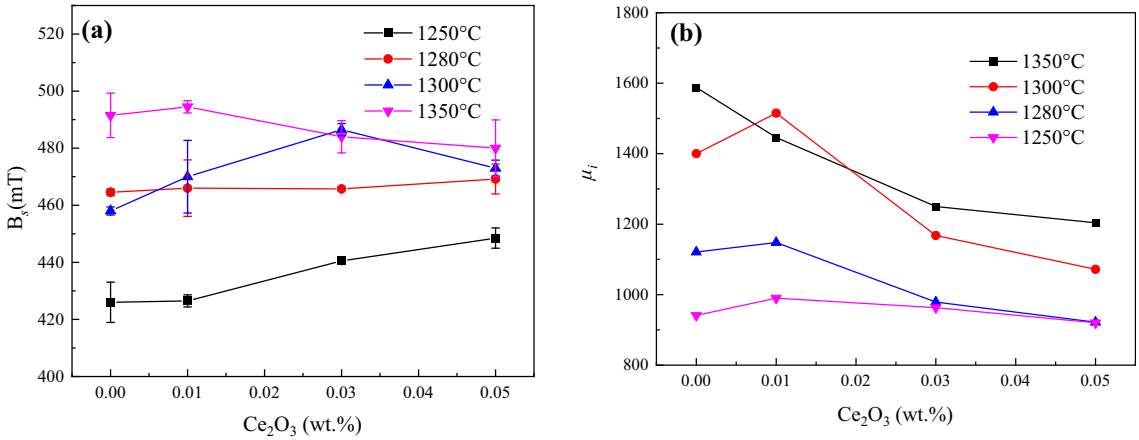

Fig. 3. The saturation magnetic induction B_s (a) and the initial permeability μ_I (b) of the Mn-Zn ferrite samples with different Ce_2O_3 doping sintered at various temperatures.

In general, the increase of μ_I with increasing grain size D results from the increase of sintering temperature. However, for the sample with identical Ce_2O_3 content, the porosity and interior stress increase drastically with the increasing sintering temperature; that is, the values of β and σ also increase. As a result, even if the grain size increases several times or even tens of times, the μ_I only increases by less than 70%. For example, for the samples without Ce_2O_3 doping, when the sintering temperature increases from 1250°C to 1350°C, the average grain size increases from 3.0–3.5 μm to 20–25 μm, which is an increase of about 800%, but the μ_I increases from 941 to 1588, which is about 68.8%.

For the samples sintered at the same temperatures of 1250°C, 1280°C, or 1300°C, the μ_I increases slightly with the addition of 0.01 wt.% Ce_2O_3, but decreases significantly with the further increase of the addition. For example, the μ_I of the sample with 0.01 wt.% Ce_2O_3 sintered at 1250°C or 1300°C is 990 or 1515, respectively, 5.2% or 8.2% higher, respectively, than that of the sample without Ce_2O_3. The reason is that a trace content of Ce_2O_3 can increase the grain size to an optimized value; however, excessive Ce_2O_3 (≥ 0.01 wt.%) reduces the value of μ_I. The reason can be attributed to, on the one hand, the non-uniform growth of the grains, and, on the other hand, the increase of impurity concentration and the interior stress due to the increase of intragrain pores, as discussed above. These results indicate that the doping with Ce_2O_3 can effectively promote grain growth, but an excessive addition of Ce_2O_3 can easily lead to a decrease of μ_I. Hence, to increase the μ_I, the approach of controlling the grain size by modifying the sintering temperature is more effective than that by doping with Ce_2O_3.

Figure 4a shows the amplitude permeability μ_a at different frequencies for the samples with different Ce_2O_3 additions sintered at various temperatures. Figure 4b shows that the high sintering temperature leads to high μ_a for the samples with identical Ce_2O_3 contents. For all the samples sintered at 1350°C, the μ_a reaches 3600–4100 at 20 kHz, which is much higher than the initial permeability of 1200–1600. In general, the μ_I is in direct proportion to the μ_a, but much lower than the μ_a. It can be demonstrated that the μ_I was measured at $B \leq 0.25$ mT, and the magnetization is dominated by the magnetic moment rotation, resulting in the low value of μ_I. However, the μ_a was measured at B = 100 mT. Under this condition, the magnetization process in the sample includes reversible domain-wall magnetization in a weak magnetic field and irreversible domain-wall displacement in a medium magnetic field, i.e., a Barkhausen jump, where the magnetization curve is in a steep part,[27] so the measured values of μ_a are much higher.

At the same sintering temperature, doping a certain amount of Ce_2O_3 effectively improves the μ_a of the sample, but, at different sintering temperatures, the optimum addition amount of Ce_2O_3 varies. At the test condition of 20 kHz and 100 mT, the μ_a increases monotonously with the addition of Ce_2O_3 (0–0.05 wt.%) at lower sintering temperatures, i.e., 1250°C or 1280°C, and it increases first and then decreases with the addition of Ce_2O_3, with a maximum value at 0.03 wt.%. Similar variation of μ_a in Co-substituted Mn-Zn ferrite has been reported before.[28] By doping 0.01 wt.% CoO, the high value of μ_a can reach 3906 at 100 kHz and 100 mT. The μ_a first increases and then decreases with the addition of Ce_2O_3 at the sintering temperature of 1350°C, with a maximum value of 0.01 wt.%. These results thus indicate that, for a lower sintering temperature, the optimum addition of Ce_2O_3 is higher. To achieve an expected high μ_a, the sintering temperature can be reduced properly by doping a certain amount of Ce_2O_3, which is beneficial for industrial production.

The above results also show that the smaller grain size leads to the lower μ_a, which is mainly attributed to the grain boundaries hindering the domain wall displacement. The fluctuation of the interior stress, impurities, and grain boundaries in

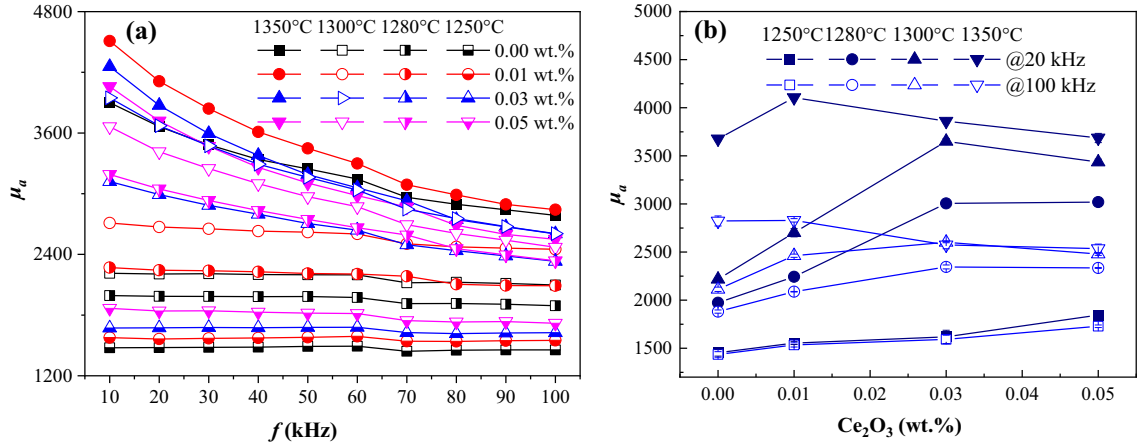

Fig. 4. The dependences of amplitude permeability on the Ce_2O_3 content at the frequencies of 20 kHz (a) and 100 kHz (b).

a magnet result in the internal energy varying with the location of the domain wall. The domain wall can be pinned in some low-energy areas, and this leads to irreversible domain wall displacement. The sample with a larger grain sizes has smaller areas of grain boundaries, which is the reason for the weaker resistance to the domain wall displacement and the higher μ_a. For the sample with small grain sizes (less than 5 μm), the domain magnetization is dominated by the magnetization rotation and hence the permeability is low. For the samples doped with Ce_2O_3 and sintered at high temperatures (1300°C and 1350°C), the lattice stress increases due to the distortion or the impurity precipitation at the grain boundaries, which offsets the effect of the increasing grain size and the decreasing grain boundary number. Therefore, the μ_a decreases with the addition of excess Ce_2O_3.

From Fig. 4a, the μ_a with the higher value at 10 kHz tends to drastically decrease with the increase of frequency. Combined with the microstructure analysis, this indicates that the larger grain size of the sample leads to a faster decrease of μ_a with the increase of frequency. The main reason is that there are more pores inside the grains and greater internal stress in the sample with larger grain sizes. When there are impurities or voids in the material, the distribution of the magnetization vector is discontinuous, and magnetic poles will be generated around the impurities or voids, forming a local demagnetization field. The domain wall locates at the center of the impurity, which is in the most stable state. If the domain wall is removed from the center of the impurity, the work of the external magnetic field is needed. The more impurities and voids in the material, the more difficult it is for the domain wall to move, and the smaller the permeability. Under an AC magnetization condition, the dynamic magnetization of the samples with more porosity and greater stress in the grains requires more work, so the μ_a decreases significantly with the increasing frequency. On the other hand, the samples with small grains are mainly domain-switching magnetized in the weak or medium magnetic fields, and are insensitive to the external pores and stress of the grains. Therefore, they have a good frequency stability of μ_a.

The magnetic loss of the Mn-Zn ferrite can be divided into three parts, i.e., hysteresis loss caused by hysteresis, eddy current loss caused by the eddy current, and residual loss caused by the magnetization relaxation process. The loss of Mn-Zn ferrite is closely related to its application frequency. It has been shown that its total loss satisfies the following formula:[29,30]

$$P_s = P_h + P_e + P_r = K_H B^3 f + K_E B^2 f^2/\rho + P_r \quad (2)$$

where P_s is the total loss, P_h is the hysteresis loss, P_e is the eddy current loss, P_r is the residual loss, B is the magnetic induction intensity, f is the frequency, ρ is the resistivity, and K_H and K_E are the hysteresis loss coefficient and the eddy current loss coefficient, respectively. Usually, the hysteresis loss is the dominant factor below 100 kHz, the eddy current loss is the dominant factor between 100 kHz and 500 kHz, and the residual loss is the dominant factor when the frequency exceeds 500 kHz.[31]

Figures 5 and 6 show the magnetic loss and coercivity, respectively, of the samples with different Ce_2O_3 contents sintered at different temperatures at various frequencies. Both figures show similar variations of the coercivity and magnetic loss. Under the test condition (100 mT, 10–100 kHz, and room temperature), the loss for all the samples increases almost linearly with the increase of frequency. This is because the hysteresis loss of Mn-Zn ferrite at low and medium saturation magnetic fields ($f \le 100$ kHz, $B \le 200$ mT) accounts for about 70% of t he total loss.[32] According to Eq. (2), the hysteresis loss is proportional to the frequency. The hysteresis loss Wa for one cycle of magnetization is equal to the area of the hysteresis loop, i.e., $Wa = \oint H \cdot dB$. The area of the hysteresis loop mainly depends on the coercivity when the specific

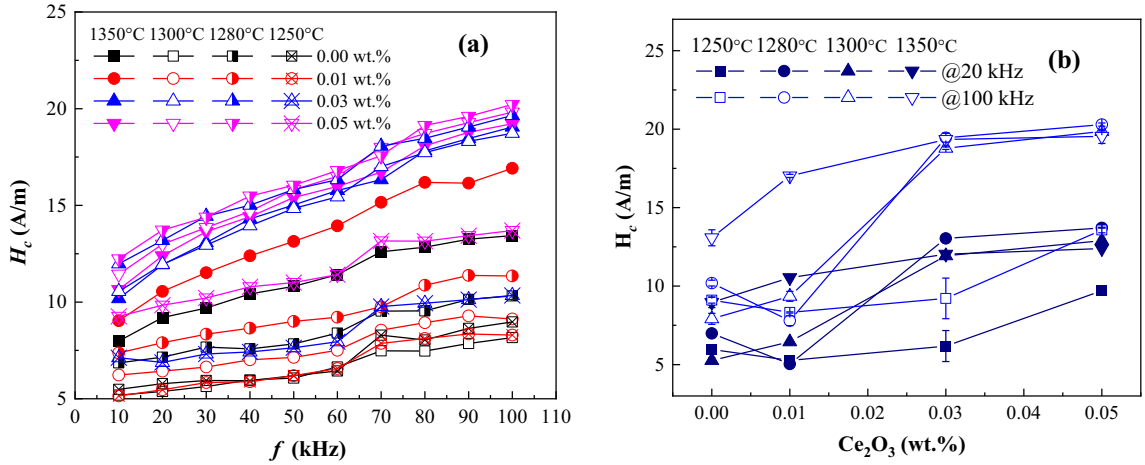

Fig. 5. Coercivity at different frequencies for the samples sintered at various temperatures: (a) 10–100 kHz; (b) 20 kHz, 100 kHz.

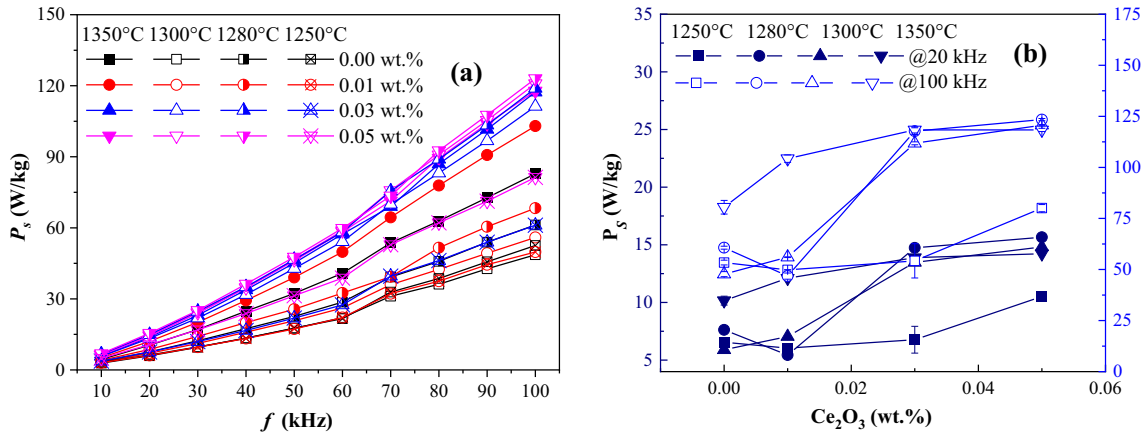

Fig. 6. Magnetic loss at different frequencies for the samples sintered at various temperatures: (a) 10–100 kHz; (b) 20 kHz, 100 kHz.

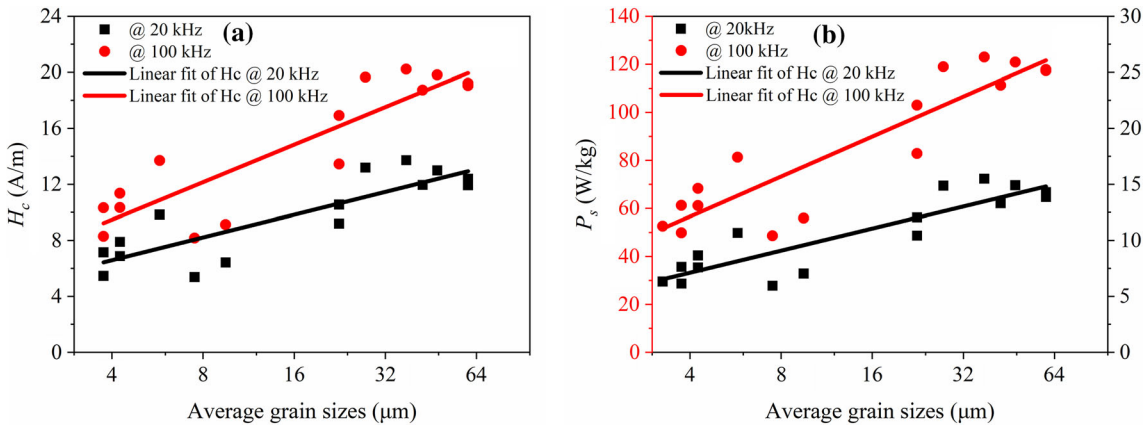

Fig. 7. Relationships between the coercivity and the average sizes (a), and the magnetic loss and the average sizes (b).

magnetic induction intensity is small. The present results thus verify that the hysteresis loss is the main loss of the ferrite in the present testing conditions.

Figures 5 and 6 also indicate that the magnetic loss and coercivity of the samples increase with the increase of sintering temperature or the addition of Ce_2O_3. Figure 7 gives the variations of the coercivity and the magnetic loss with the average grain

size, showing that both the coercivity and the magnetic loss have a tendency to increase with the increasing grain size. Roughly, when the grain size is less than 25 μm, the magnetic loss and coercivity only increase slightly with the grain size. The reason is that the coercivity of the sample depends mainly on the size and distribution of the pores in the grains and the stress. Hu et al.[33] also reported that, for the Ni-Zn ferrite co-doping with 0.4 wt.% V_2O_5 and 0.1 wt.% $MnCO_3$, the minimum value of P_{cv}= 393.6 kW/m^3 can be reached at a sintering temperature of 1100°C. Excessive doping and sintering temperature led to the increase of the grain size and the increasing P_{cv}. When the grain size is larger than 25 μm, the pores are basically existing in the grains for all the samples, and the sizes and distribution of the pores are similar. As a result, the coercivity and the magnetic loss are more dependent on the grain size.

The above results reveal that, by doping a certain amount of Ce_2O_3 and controlling the sintering temperature, enhanced magnetic properties, such as high B_s, high μ_a with excellent frequency stability, and low P_s, can be obtained. The high values of B_s = 495 mT and μ_a = 4105 (20 kHz, 100 mT) can be achieved in the sample doped with 0.01 wt.% Ce_2O_3 and sintered at 1350°C, and the minimum of P_s = 5.4 W/kg can be obtained in the sample doped with 0.01 wt.% Ce_2O_3 and sintered at 1280°C. These characteristics are beneficial for the magnetic core used in electromagnetic induction heating systems. The high B_s and low power loss can ensure a high power conversion efficiency, and the high μ_a with excellent frequency stability can ensure a high stability during the working process of the heating system. In addition, Ce-doped Mn-Zn ferrites also show great potential for other applications, such as inductors and transformers.

CONCLUSIONS

The effects of Ce_2O_3 doping and sintering temperature on the microstructure and magnetic properties of Mn-Zn ferrites prepared by a conventional ceramic process have been studied in order to optimize their magnetic performance. The results show that all the samples sintered at 1250–1350°C have reacted completely to form a spinel ferrite phase. Doping 0.05 wt.% $CaCO_3$ and 0–0.05 wt.% Ce_2O_3 has no significant effect on the lattice structure, while Ce_2O_3 addition can effectively promote the grain growth. The distribution of the pores has important effects on the magnetic properties. For the samples with grain sizes less than 10 μm, the pores are mainly distributed at the grain boundary, especially at the junction of triple grains. For those with grains larger than 10 μm, the pores appear inside the grains. With the same addition of Ce_2O_3, the initial permeability increases with the increase of sintering temperature. Doping excessive Ce_2O_3 ($\geq$ 0.03 wt.%) leads to a significant decrease of the initial permeability. A high sintering temperature leads to a high amplitude permeability for the sample with the same Ce_2O_3 content. The magnetic loss and coercivity increase with the increase of the sintering temperature or the addition of Ce_2O_3. The present results have demonstrated that a certain amount of Ce_2O_3 doping is beneficial for the soft magnetic properties of MnZn ferrites if the sintering temperature can be well controlled. Ce-doping of Mn-Zn ferrites show great potential for applications in induction heating systems and other fields.

ACKNOWLEDGMENTS

This work was partly supported by the Sanqiaohui (Foshan) New Materials Co., Ltd. and the Foshan Midea Galvanothermy Electric Appliances Co., Ltd.

CONFLICT OF INTEREST

The authors declare that they have no conflict of interest.

REFERENCES

1. R. Valenzuela, *J. Am. Chem. Soc.* 118, 5 (1994).
2. K.I. Arshak, A. Ajina, and D. Egan, *Microelectron. J.* 32, 113 (2001).
3. K. Arshaka, K. Twomey, and D. Egan, *Sensors* 2, 50 (2002).
4. A. Zapata and G. Herrera, *Ceram. Int.* 39, 7853 (2013).
5. K.Q. Jiang, K.K. Li, C.H. Peng, and Y. Zhu, *J. Alloys Compd.* 541, 472 (2012).
6. X.C. Zhong, X.J. Guo, S.Y. Zou, H.Y. Yu, Z.W. Liu, Y.F. Zhang, and K.X. Wang, *AIP Adv.* 8, 047807 (2018).
7. J. Jiang, L.C. Li, and F. Xu, *J. Rare Earth* 25, 79 (2007).
8. L.J. Zhao, H. Yang, L.X. Yu, Y.M. Cui, and S.H. Feng, *J. Mater. Sci.* 41, 3083 (2006).
9. D.Y. Li, Y.K. Sun, Y. Xu, H.L. Ge, Q. Wu, and C. Yan, *Ceram. Int.* 41, 4581 (2015).
10. N. Boda, G. Boda, K.C.B. Naidu, M. Srinivas, K.M. Batoo, D. Ravinder, and A.P. Reddy, *J. Magn. Magn. Mater.* 473, 228 (2019).
11. P.P. Naik, R.B. Tangsali, S.S. Meena, and S.M. Yusuf, *Mater. Chem. Phys.* 191, 215 (2017).
12. D.O. Alikin, A.P. Turygin, J. Walker, A. Bencan, B. Malic, T. Rojac, V.Y. Shur, and A.L. Kholkin, *Acta Mater.* 125, 265 (2017).
13. X.F. Wu, Z. Ding, N.N. Song, L. Li, and W. Wang, *Ceram. Int.* 42, 4246 (2016).
14. S.L. Ahmad, S.A. Ansari, and D. Ravi Kumar, *Mater. Chem. Phys.* 208, 248 (2018).
15. L.C. Li, J. Jiang, and F. Xu, *Mater. Lett.* 61, 1091 (2007).
16. F. Falsafi, B. Hashemi, A. Mirzaei, E. Fazio, F. Neri, N. Donato, S.G. Leonardi, and G. Neri, *Ceram. Int.* 43, 1029 (2017).
17. J. Wei, C.F. Wu, Y.L. Liu, Y.X. Guo, T.T. Yang, D.W. Wang, Z. Xu, and R. Haumont, *Inorg. Chem.* 56, 8964 (2017).
18. E. Rezlescu, N. Rezlescu, P.D. Popa, L. Rezlescu, and C. Pasnicu, *Phys. Status Solidi A* 162, 673 (1997).
19. B.P. Jacob, S. Thankachan, S. Xavier, and E.M. Mohammed, *J. Alloys Compd.* 578, 314 (2013).
20. M. Rahimi-Nasrabadi, M. Behpour, A. Sobhani-Nasab, and R.J. Mansoureh, *J. Mater. Sci. Mater. Electron.* 27, 11691 (2016).
21. C. Sun and K.N. Sun, *Solid State Commun.* 141, 258 (2007).
22. C. Sun, K.N. Sun, and P.F. Chui, *J. Magn. Magn. Mater.* 324, 802 (2012).
23. C.S.L.N. Sridhar, K.S.S.M. Laxmi, D.M. Potukuchi, and C.S. Lakshmi, *Mater. Res. Express* 6, 126117 (2020).

24. M.M.L. Sonia, S. Anand, V.M. Vinosel, M. Asisi Janifer, and S. Pauline, *J. Mater. Sci. Mater. Electron.* 29, 15006 (2018).
25. M.A. Dar, K. Majid, M. Hanief Najar, R.K. Kotnala, J. Shah, S.K. Dhawan, and M. Farukh, *Phys. Chem. Chem. Phys.* 19, 10629 (2017).
26. M.F. Yan and D.W. Johnson Jr, *J. Am. Ceram. Soc.* 61, 342 (1978).
27. D.F. Wan and X.L. Ma, *Magnetic physics (Revised Edition)* (Beijing: Beijing Electronic Industry Press, 1999), pp. 213–388.
28. C. Beatrice, S. Dobák, V. Tsakaloudi, C. Ragusa, F. Fiorillo, L. Martino, and V. Zaspalis, *AIP Adv.* 8, 047803 (2018).
29. Y.P. Liu and S.J. He, *J. Magn. Magn. Mater.* 320, 3318 (2008).
30. A.H. Taghvaei, H. Shokrollahi, K. Janghorban, and H. Abiri, *Mater. Des.* 30, 3989 (2009).
31. D. Liu, X.P. Chen, Y. Ying, L. Zhang, W.C. Li, L.Q. Jiang, and S.L. Che, *Ceram. Int.* 42, 9152 (2016).
32. C. Beatrice, O. Bottauscio, M. Chiampi, F. Fiorillo, and A. Manzin, *J. Magn. Magn. Mater.* 304, e743 (2006).
33. D.W. Hu, F. Zhao, L. Miao, Z. Zhang, Y. Wang, H.L. Cheng, Y.F. Han, M.J. Tian, H.X. Gu, and R. Ma, *Ceram. Int.* 45, 10028 (2019).